



LAWRENCE  
LIVERMORE  
NATIONAL  
LABORATORY

# The Urbach tail in silica glass from first principles

B. Sadigh, P. Erhart, D. Aberg, A. Trave, E.  
Schwegler, J. Bude

June 17, 2010

Physical Review Letters

## **Disclaimer**

---

This document was prepared as an account of work sponsored by an agency of the United States government. Neither the United States government nor Lawrence Livermore National Security, LLC, nor any of their employees makes any warranty, expressed or implied, or assumes any legal liability or responsibility for the accuracy, completeness, or usefulness of any information, apparatus, product, or process disclosed, or represents that its use would not infringe privately owned rights. Reference herein to any specific commercial product, process, or service by trade name, trademark, manufacturer, or otherwise does not necessarily constitute or imply its endorsement, recommendation, or favoring by the United States government or Lawrence Livermore National Security, LLC. The views and opinions of authors expressed herein do not necessarily state or reflect those of the United States government or Lawrence Livermore National Security, LLC, and shall not be used for advertising or product endorsement purposes.

# The Urbach tail in silica glass from first principles

B. Sadigh, P. Erhart, D. Åberg, A. Trave, E. Schwegler, and J. Bude

Lawrence Livermore National Laboratory, Chemistry, Materials and Life Sciences Directorate, Livermore, CA, 94550

(Dated: June 15, 2010)

We present density-functional theory calculations of the optical absorption spectra of silica glass for temperatures up to 2400 K. The calculated spectra exhibit exponential tails near the fundamental absorption edge that follow the Urbach rule, in quantitative agreement with experiments. We discuss the accuracy of our results by comparing to hybrid exchange correlation functionals. We derive a simple relationship between the exponential tails of the absorption coefficient and the electronic density-of-states, and thereby establish a direct link between the photoemission and the absorption spectra near the absorption edge. We use this relationship to determine the lower bound to the Urbach frequency regime. We show that in this frequency interval, the optical absorption is Poisson distributed with very large statistical fluctuations. We determine the upper bound to the Urbach frequency regime by identifying the frequency at which transition to Poisson distribution takes place.

At finite temperatures, the absorption spectra of insulators can be modified substantially through interaction of the electronic states with lattice vibrations. In 1953 Urbach observed an exponential energy dependence of the absorption coefficient near the fundamental absorption edge that varied with temperature as follows

$$\bar{\alpha}(\omega, T) = \alpha_0 \exp \left[ -\sigma \frac{\hbar\omega_0(T) - \hbar\omega}{kT} \right]. \quad (1)$$

Here  $\omega_0(T)$  is a linear function of temperature, which at zero K is defined to be the optical gap and  $\sigma$  and  $\alpha_0$  are constants that can be extracted from experiments. The so-called Urbach rule described by Eq. (1), has been observed universally in crystals as well as glasses, in both semiconductors and insulators. The physical origin of the Urbach rule has been discussed extensively over the years [1–3]. At this point there is consensus that it corresponds to transitions between localized electronic levels that result from temporal fluctuations of the band-edge electrons into the band gap, and extended band-like states. Since Urbach behavior involves electron localization [4, 5] in the presence of vibrations, it is not obvious that standard electronic structure theories such as the density-functional theory (DFT) in the local-density (LDA) or gradient-corrected (GGA) approximations can capture these effects, in particular when considering their systematic underestimation of band gaps of insulators. In a pioneering work, Drabold *et al.* performed *ab initio* LDA molecular-dynamics (MD) simulations of amorphous Si and calculated the fluctuations in the single-particle eigenvalues at the band edges [6]. When comparing with the photoemission spectra, they obtained good agreement. This showcased the applicability of *ab initio* MD in the adiabatic approximation within LDA to describe the electronic structure of semiconductors at finite temperatures. However, the quantitative computation of the Urbach tail of the optical absorption remains a daunting task. It requires calculating the probability distribution of rare dipole transition events, which necessitates long-time *ab initio* MD simulations in order to obtain the time-dependent fluctuations of the single-particle eigenvalues and the dipole matrix elements. In the past, almost invariably the assumption has been made that the latter do not vary appreciably with atomic displacements or frequency, an assumption that is very difficult to justify specially at high temperatures.

In this paper, we investigate the Urbach rule in silica glass using *ab initio* MD simulations. This has been motivated by the need to develop a better understanding of the process of laser damage to silica optics, of importance to diverse fields from telecommunications to inertial confinement fusion. In the past, much computational work has been directed to studying zero K absorption due to defects in silica [7–9]. Recently, the role of temperature has been emphasized by experiments where damage was generated far below the bulk material threshold by photons of energy 3.55 eV when silica was heated to about 2200 K [10]. The Urbach rule plays a crucial role here since the exponential dependence of absorption on temperature in Eq. (1), necessitates the existence of a critical temperature  $T_c$ , at which the glass absorbs more photon energy than it can dissipate. However, extrapolation to higher temperatures of the experimental spectra available up to 1900 K cannot quantitatively reproduce the measured  $T_c$ . Therefore better understanding of the kinetics of absorption at finite temperatures in the Urbach regime is needed. Our purpose here is to study the intrinsic absorption in silica at finite temperatures, validate the *ab-initio* MD approach with the existing experimental data, and then investigate the physics of absorption in the Urbach tail, where accurate experiments are not available.

The MD simulations presented in this work are performed within the DFT-GGA framework using the PW91 parametrization [11, 12] as implemented in the Vienna *ab-initio* simulation package [13–16] using the projector augmented wave method [17, 18]. All calculations involve supercells containing 24 SiO<sub>2</sub> formula units and the Brillouin zone is sampled by a  $2 \times 2 \times 2$  Monkhorst-Pack  $k$ -point grid. In order to obtain a realistic glass model, we started from a liquid silica model obtained previously [19], which was quenched down to zero K over a period of about 10 ps. The examination of the electronic structure of the resulting glass model revealed several defect states due to the presence of a few stretched and broken bonds. The defect states were eliminated from the model by optimizing it using a bond-switching Monte Carlo (BSMC) technique [20]. Several BSMC-refined configurations were generated, each representing a random network with perfect bond lengths and angles. Subsequently, the configurations were structurally relaxed to the local GGA total energy minimum. The final glass model that was cho-

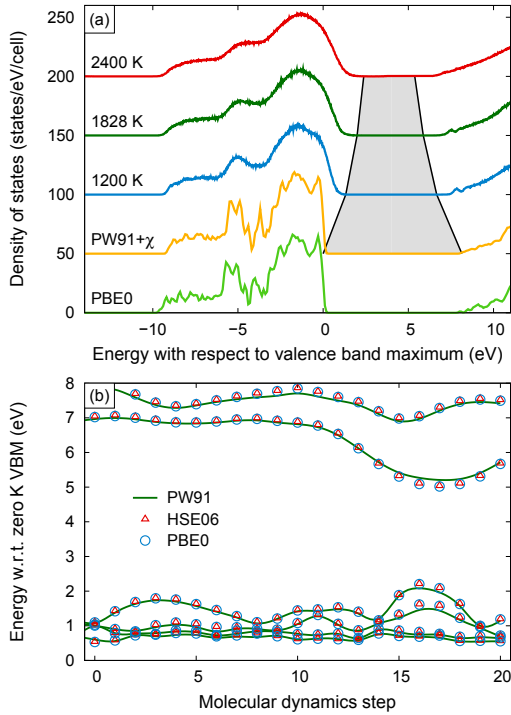


FIG. 1: (a) Density-of-states for the perfect glass at zero K calculated using the PBE0 hybrid functional (lowermost line) and the PW91 functional with scissors correction (PW91+ $\chi$ , second line from the bottom). Also shown is the density of states for three different non-zero temperature obtained from MD simulations using PW91+ $\chi$ . (b) Eigenenergies for a number of configurations along an MD trajectory obtained using two different hybrid functionals (HSE06, PBE0) in comparison with the PW91+ $\chi$  approach.

sen from this set had preserved its bond lengths and angles after the relaxation process. The electronic density-of-states (DOS) of this configuration as well as  $\alpha$ -quartz are shown in 1(a), where comparison is made with the PBE0 hybrid functional which includes 25% exact exchange [21–24]. The GGA DOS includes a band-gap shift of  $\Delta_g = 2.6$  eV in order to compare with the PBE0 results. Note the great agreement between the two calculations. This is not surprising. In general it is expected that GGA-DFT, except for the band gap, can reproduce most of the features of the electronic structure of insulators accurately. However, as mentioned earlier, the electronic eigenstates at the band edges undergo localization when they fluctuate inside the band gap. If the band gap shift depends strongly on the degree of localization of these states, then GGA-DFT is fundamentally incapable of a quantitative prediction of the Urbach tail. We have addressed this issue by explicitly comparing the time evolution of the band edge states at 2200 K, calculated from GGA with PBE0 as well as HSE06 [25] (a hybrid functional that includes screened exchange), see Fig. 1(b). It appears that with a constant band gap shift (2.6 eV for GGA and 0.9 eV for HSE06), all calculations can be brought in agreement with each other. We thus conclude that DFT-GGA provides a reasonable basis for modeling the Urbach tail from first principles. A similar con-

clusion was reached by Alkauskas *et al.* in studying point defects [9].

The absorption coefficient for photons of energy  $\hbar\omega$  of an atomic configuration  $\mathbf{X}$ , can be calculated as follows

$$\alpha(\omega; \mathbf{X}) = \sqrt{2} \frac{\omega}{c} \sqrt{|\epsilon(\omega; \mathbf{X})| - \epsilon_R(\omega; \mathbf{X})}, \quad (2)$$

where  $\epsilon(\omega; \mathbf{X})$  is the complex dielectric function:  $\epsilon = \epsilon_R + i\epsilon_I$ . In the velocity gauge,  $\epsilon_I$  can be directly computed from the single-particle wave functions, eigenvalues [26, 27] and their occupancies  $f_{n\mathbf{k}}$  as follows

$$\epsilon_I(\omega; \mathbf{X}) = \frac{4\pi^2 e^2}{m_e^2 \omega^2} \sum_{n,n'} (f_{n'\mathbf{k}} - f_{n\mathbf{k}}) |M_{nn'}^{\mathbf{k}}(\mathbf{X})|^2 \times \delta(\Delta_g + e_{n'\mathbf{k}}(\mathbf{X}) - e_{n\mathbf{k}}(\mathbf{X}) - \hbar\omega), \quad (3)$$

where  $M_{nn'}^{\mathbf{k}}(\mathbf{X})$  are the polarization-averaged dipole matrix elements between the states  $n\mathbf{k}$  in the valence band and  $n'\mathbf{k}$  in the conduction band. The sums in Eq. (3) run over all the bands and spins. The real part  $\epsilon_R$  can be obtained from  $\epsilon_I$  through a Kramers-Kronig relation. Since this involves an integration over the entire frequency spectrum, we have included as many as 1000 unoccupied bands in our calculations in order to obtain accurate values for  $\epsilon_R$ .

At finite temperatures, the response functions as well as the DOS are calculated by classical ensemble averaging over ionic displacements in the Born-Oppenheimer approximation, which amounts to averaging over the MD simulation time steps. In this way, the electronic transitions are treated as instantaneous. The finite-temperature electronic state occupancies are determined by the Fermi-Dirac distribution  $f_{n\mathbf{k}} = 1 / \left( 1 + \exp\left(\frac{e_{n\mathbf{k}} - \mu(T)}{kT}\right) \right)$ . The electronic chemical potential  $\mu(T)$  is calculated from the charge neutrality condition,  $\int_{-\infty}^{\mu(T)} \langle \rho(\epsilon) \rangle_T d\epsilon = N_e$ , where  $N_e$  is the total number of electrons, and  $\langle \rho(\epsilon) \rangle_T$  is the average DOS. Figure 1(a) shows the average DOS at three different temperatures. The gray region depicts the band-gap narrowing with increasing temperature. This contributes to creating holes and electrons in the valence and the conduction bands. The equilibrium concentrations of free electrons as a function of temperature can be calculated by summing up the total occupancies of the conduction band states. Although the free electron concentration is as large as  $10^{-17} \text{cm}^{-3}$  at 2400 K, it is still too small to have any measurable impact on the absorption coefficients in the Urbach regime, i.e. the latter can be calculated with no loss of accuracy with zero K occupancies. The connection to absorption from the DOS is through the joint density-of-states (JDOS), which for zero K occupancies can be defined as  $J(\omega) = \int \rho_v(\omega') \rho_c(\omega' + \omega) d\omega'$ , where  $\rho_{v(c)}(\omega)$  is the DOS of the occupied (unoccupied) bands. At finite temperatures, a direct relationship between the JDOS and the DOS only exists if the fluctuations in the valence and the conduction bands were independent

$$\langle \mathcal{J}(\omega) \rangle_T \approx \int \langle \rho_v(\omega') \rangle_T \langle \rho_c(\omega' + \omega) \rangle_T d\omega'. \quad (4)$$

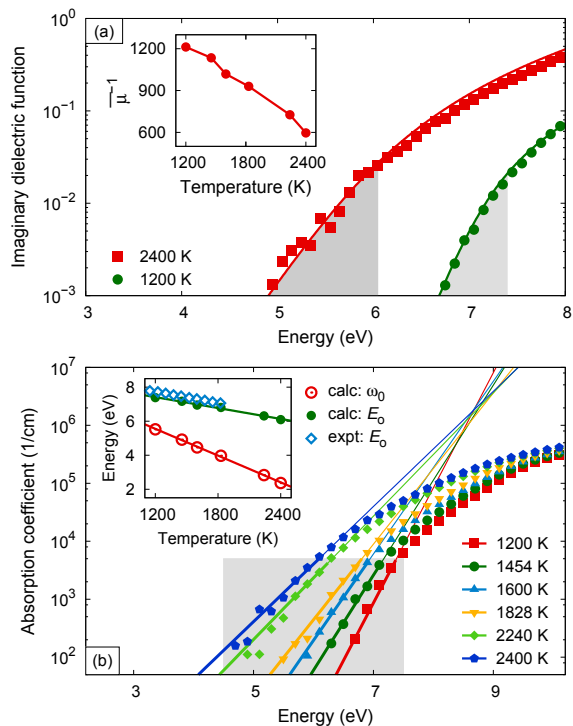


FIG. 2: (a) Joint-density-of-states and imaginary dielectric function at two different temperatures calculated from MD simulations. The inset shows the free electron concentration as a function of temperature. (b) Absorption coefficient in the Urbach regime at different temperatures calculated from MD simulations using the PW91 functional with a scissors shift. The inset shows the result of the fit to Eq. (1) and the comparison with the experimental data from Saito and Ikushima [28].

We find that the above is a very good approximation at all frequencies  $\omega$ . This is illustrated in Fig. 2(a), where the structure of the low-frequency exponential tail of the JDOS at several temperatures can be observed. We also show the imaginary dielectric function in the same figure. This was made possible through rescaling the JDOS with a temperature-dependent effective dipole transition probability  $\bar{\mu}(T)$  to fit the low-frequency exponential tails of the imaginary dielectric function.

$$\langle \epsilon_I(\omega) \rangle_T \approx \bar{\mu}(T) \langle \mathcal{J}(\omega) \rangle_T. \quad (5)$$

Note how well these tails are reproduced by the JDOS over the entire temperature range. This is an important result, which suggests that the matrix elements are not necessary to reproduce the frequency dependence of the low-energy exponential tail of the dielectric function. However, they cannot be neglected entirely, since they lead to an effective temperature-dependent coefficient that changes by a factor of two between 1200 and 2400 K. In the inset of Fig: 2(a), we show that  $\bar{\mu}^{-1}(T)$  decreases linearly with increasing temperature.

We now proceed to calculate the absorption spectra using Eq. (2), for temperatures ranging from 1200 to 2400 K as shown in Fig. 2(b). Simultaneously fitting the low-energy exponential tails of the calculated spectra at all temperatures to

Eq. (1), yields  $\sigma = 0.473$  and the values of  $\omega_0(T)$  shown in the inset of Fig. 2(b). The latter is very well approximated by a linear function of temperature,  $\omega(T) = 8.70 \text{ eV} - T \cdot 1.07 \times 10^{-3} \text{ eV/K}$ . This result is in accordance with Urbach's rule and is in excellent agreement with the experiments by Saito and Ikushima [28], where  $\sigma = 0.585$  and  $\omega(T) = 8.76 \text{ eV} - T \cdot 1.01 \times 10^{-3} \text{ eV/K}$ . Both the experimental [28] and calculated Tauc gap energies are shown in the inset in Fig. 2(b). We have followed Saito and Ikushima [28] and defined the Tauc gap as the photon energy corresponding to  $5 \times 10^3 \text{ cm}^{-1}$  absorption. The calculated linear temperature dependence of  $\omega_0(T)$  in Fig. 2(b) extends the Urbach rule up to 2400 K. However, for the system size and simulation times considered here, our glass model remains a vibrating system. The effect of melting and diffusion on the Urbach rule is outside the scope of this work. This result is still valuable for modeling run-away absorption where explosive heating occurs over very short time scales.

It is interesting to note that in the Urbach regime the ratio  $\langle \epsilon_I(\omega) \rangle_T / \langle \epsilon_R(\omega) \rangle_T \ll 1$ . A first order Taylor expansion of Eq. (2) with respect to this quantity yields the following expressions for the absorption coefficient

$$\langle \alpha(\omega) \rangle_T \approx \frac{\omega}{c} \frac{\langle \epsilon_I(\omega) \rangle_T}{\sqrt{\langle \epsilon_R(\omega) \rangle_T}} \approx \frac{\omega \bar{\mu}(T) \langle \mathcal{J}(\omega) \rangle_T}{c \sqrt{\langle \epsilon_R(0) \rangle_T}}. \quad (6)$$

The second approximation above is obtained by a zeroth order expansion about the static dielectric constant  $\langle \epsilon_R(0) \rangle_T$ , and utilizes our earlier finding that the Urbach tail of the imaginary dielectric function can be obtained from the JDOS, see Eq. 5. Using the above together with Eq. (4), we can thus establish a simple relationship between the absorption coefficient and the DOS in the vicinity of the absorption edge, where the temperature dependence of the prefactor is mainly through the effective oscillator strengths  $\bar{\mu}(T)$ , while  $\langle \epsilon_R(0) \rangle_T$  varies only weakly with temperature, i.e. from 1.81 at 0K to 1.99 at 2400 K, corresponding to an increase of less than 10% over 2400 K. We point out that the DOS is obtained experimentally through photoemission spectroscopy. Therefore, the above result provides a direct link between the photoemission and the optical absorption experiments in the Urbach tail region of the spectrum.

Equation (6) has the important implication that at finite temperatures the dipole matrix elements average out such that in the Urbach tail they can be replaced by a temperature-dependent prefactor. The atomic vibrations also lead to significant statistical fluctuations, which at this point is computationally very expensive for us to quantify accurately. However, we can use Eq. (6) to obtain a lower bound on the statistical fluctuations in  $\alpha(\omega)$  by neglecting the fluctuations in the matrix elements and study  $\langle \mathcal{J}^2(\omega) \rangle_T$ . This is shown in Fig. 3a), where comparison is made with  $\langle \mathcal{J}(\omega) \rangle_T^2$ . A significant departure between the two curves is seen in the Urbach tail, where the ratio  $Q(\omega) = \langle \mathcal{J}^2(\omega) \rangle_T / \langle \mathcal{J}(\omega) \rangle_T^2$  can reach  $10^4$ . Hence the standard deviation from mean absorption for frequencies in the Urbach tail is more than an order of magnitude larger than  $\langle \alpha(\omega) \rangle_T$ .

The origin of the large fluctuations in the Urbach regime

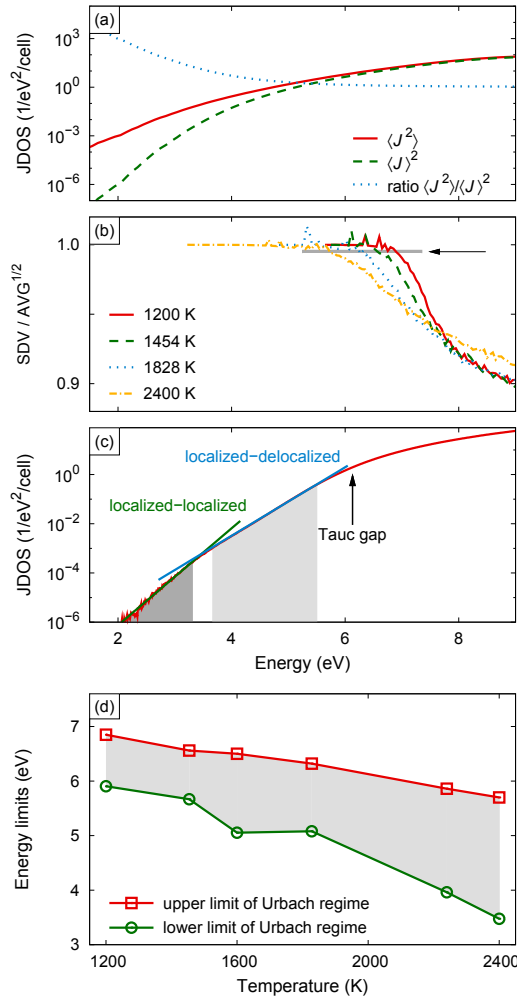


FIG. 3: (a) First and second moment of the joint density of states (JDOS) as well as their ratio at 2400 K. (b) In the Urbach regime The standard deviation of the JDOS equals the square root of the average indicative of a Poisson distribution. The energy at which the ratio deviates from one provides a simple measure for the upper limit of the Urbach regime as indicated by the arrow. (c) At low energies, the JDOS exhibits two distinct regions corresponding to localized-delocalized (Urbach regime) and localized-localized transitions. Each region is described by a different exponential the crossing point of which defines a lower limit for the Urbach regime. Note that the Tauc gap lies above the region within which the JDOS exhibits exponential tails. (d) Upper and lower limits of the Urbach regime extracted from the data presented in (b) and (c).

lies with the discrete nature of the JDOS itself. Even if  $\langle \mathcal{J}(\omega) \rangle_T \ll 1$ , at each instant of time there can only exist an integer number  $\mathcal{N}$  of pairs of electronic states available for transition or none. Hence the absorption coefficient locally fluctuates between zero and  $\bar{\mu}^2 \times \mathcal{N}$ , which can amount to fluctuations much larger than the mean value  $\langle \mathcal{J} \rangle_T$  itself. This is a consequence of the quantum nature of matter. Let us now

define an absorption event as the instant of time when  $\mathcal{N} > 0$ . Whenever absorption events occur so rarely that they can be considered independent, the absorption process is Poisson distributed, with  $\langle \mathcal{J}(\omega) \rangle_T$  interpreted as the average rate of occurrence. An important signature of the Poisson distribution is that its standard deviation is equal to the square root of its average. Figure 3(b) shows the ratio between these two quantities for JDOS as a function of  $\omega$  for several temperatures. We see that in the Urbach regime, the equality between two quantities hold, while at higher frequencies their ratio starts deviating from one. In fact, we may define the frequency  $\omega_U$  below which the statistics becomes Poisson distributed. This frequency signifies the upper bound to the Urbach tail region of the spectrum. Figure 3(d) shows that above 1200 K,  $\omega_U$  decreases linearly with increasing This result bestows the finite-temperature JDOS in the Urbach tail with distinct physical significance. It represents the average rate of occurrence of absorption events in this frequency interval. Although there are no experiments that can directly measure JDOS, it can be determined via Eq. (4) from the finite-temperature DOS, which can be obtained from photoemission experiments. The Urbach tail region is a closed frequency interval in the optical spectrum. Above, we have determined the upper bound for this interval. We can also determine its lower bound using Eq. (4) to compute  $\langle \mathcal{J}(\omega) \rangle_T$  down to very small values with good statistical accuracy. Figure 3(c) shows that at very low energies there is a transition in the signature exponential decay of the Urbach tail to a steeper decay curve. The frequency  $\omega_L$  at which this transition occurs can be used to signify the lower bound of the Urbach region. The temperature dependence of  $\omega_L$  is shown in Fig. 3(d). The optical transitions in this lower-frequency region correspond to transitions between the localized levels in the exponential tails of the valence and the conduction bands. In contrast the Urbach tail originates from transitions between localized tail states and extended band-like states.

Finally, let us discuss the impact of the above findings on the modeling of laser heating in silica. To lowest order, laser heating can be described by a heat conduction equation with a source term that incorporates energy deposition by linear coupling to the laser  $\bar{\alpha}(\omega, T) I(\mathbf{r})$ , where  $I(\mathbf{r})$  is the laser light intensity. Neglecting fluctuations, this term can be parametrized by  $\bar{\alpha}(\omega, T) = \langle \alpha(\omega) \rangle_T$ . However, the rare event nature of absorption in the Urbach regime calls for  $\bar{\alpha}(\omega, T)$  to be treated as a time and space-dependent Poisson process, where at a rate of  $\langle \mathcal{J}(\omega) \rangle_T$  an absorption event with the strength of  $\frac{\omega}{c} \frac{\bar{\mu}^2}{\sqrt{\langle \epsilon_R(0) \rangle_T}}$  with the duration of 5 fs takes place. The spatial extent of each event is  $\approx 1$  nm, as compared with a typical laser spot of about 200 nm lasting several nanoseconds.

This work performed under the auspices of the U.S. Department of Energy by Lawrence Livermore National Laboratory under Contract DE-AC52-07NA27344 with support from the Laboratory Directed Research and Development Program.

[1] T. H. Keil, Phys. Rev. **144**, 582 (1966).

[2] C. M. S. M. H. Cohen and E. N. Economou, Phys. Rev. Lett.

- 53**, 616 (1984).
- [3] B. I. Halperin and M. Lax, Phys. Rev. **148**, 722 (1966).
- [4] T. A. Abtew and D. A. Drabold, Phys. Rev. B **75**, 045201 (2007).
- [5] Y. Pan, F. Inam, M. Zhang, and D. A. Drabold, Phys. Rev. Lett. **100**, 206403 (2008).
- [6] D. A. Drabold, P. A. Fedders, S. Klemm, and O. F. Sankey, Phys. Rev. Lett. **67**, 2179 (1992).
- [7] G. Pacchioni and G. Ieranó, Phys. Rev. B **56**, 730 (1997).
- [8] T. Bakos, S. N. Rashkeev, and S. T. Pantelides, Phys. Rev. B **70**, 075203 (2004).
- [9] A. Alkauskas, P. Broqvist, and A. Pasquarello, Phys. Rev. Lett. **101**, 046405 (2008).
- [10] J. Bude, G. Guss, M. Matthews, and M. L. Spaeth, SPIE proceedings **6720**, 672009 (2007).
- [11] J. P. Perdew and Y. Wang, Phys. Rev. B **33**, 8800 (1986).
- [12] J. P. Perdew, in *Electronic structure of solids*, edited by P. Ziesche and H. Eschrig (Akademie Verlag, Berlin, 1991), p. 11.
- [13] G. Kresse and J. Hafner, Phys. Rev. B **47**, 558 (1993).
- [14] G. Kresse and J. Hafner, Phys. Rev. B **49**, 14251 (1994).
- [15] G. Kresse and J. Furthmüller, Phys. Rev. B **54**, 11169 (1996).
- [16] G. Kresse and J. Furthmüller, Comput. Mater. Sci. **6**, 15 (1996).
- [17] P. E. Blöchl, Phys. Rev. B **50**, 17953 (1994).
- [18] G. Kresse and D. Joubert, Phys. Rev. B **59**, 1758 (1999).
- [19] A. Trave, P. Tangney, S. Scandolo, A. Pasquarello, and R. Car, Phys. Rev. Lett. **89**, 245504 (2002).
- [20] F. Wooten, K. Winer, and D. Weaire, Phys. Rev. Lett. **54**, 1392 (1985).
- [21] J. P. Perdew, K. Burke, and M. Ernzerhof, Phys. Rev. Lett. **77**, 3865 (1996), erratum, *ibid.* **78**, 1396(E) (1997).
- [22] M. Ernzerhof, J. P. Perdew, and K. Burke, Int. J. Quantum Chem. **64**, 285 (1997).
- [23] M. Ernzerhof and G. E. Scuseria, J. Chem. Phys. **110**, 5029 (1999).
- [24] C. Adamo and V. Barone, J. Chem. Phys. **116**, 6158 (1999).
- [25] J. Heyd, G. E. Scuseria, and M. Ernzerhof, J. Chem. Phys. **118**, 8207 (2003), erratum: *ibid.* **124**, 219906 (2006).
- [26] R. Del Sole and R. Girlanda, Phys. Rev. B **48**, 11789 (1993).
- [27] Z. H. Levine and D. C. Allan, Phys. Rev. B **43**, 4187 (1991).
- [28] K. Saito and A. J. Ikushima, Phys. Rev. B **62**, 8584 (2000).